Analytica Chimica Acta 1170 (2021) 338630

Contents lists available at ScienceDirect

Analytica Chimica Acta

journal homepage: www.elsevier.com/locate/aca

Smartphone-assisted point-of-care colorimetric biosensor for the detection of urea via pH-mediated AgNPs growth

Cheol-Kyun Choi [a, c, 1], Samy M. Shaban [a, b, d, 1], Byeong-Seok Moon [a], Do-Gi Pyun [c], Dong-Hwan Kim [a, b, *]

[a] School of Chemical Engineering, Sungkyunkwan University (SKKU), Suwon 16419, Republic of Korea
[b] Biomedical Institute for Convergence at SKKU (BICS), Sungkyunkwan University (SKKU), Suwon 16419, Republic of Korea
[c] Biomedical Polymer R&D Institute, T&L Co., Ltd, Anseong 17554, South Korea
[d] Petrochemicals Department, Egyptian Petroleum Research Institute, Egypt

HIGHLIGHTS

- A fast-acting, reliable smartphone-assisted colorimetric urea biosensor.
- High sensitivity of LOD as low as 0.0036 mM and high reliability of 99% ± 2.9%.
- High selectivity against various interferents in human urine.
- Paper-based smartphone-assisted POC was applied for urea sensing in human urine.
- A potential POC monitoring systems of renal and hepatic dysfunction diseases.

GRAPHICAL ABSTRACT

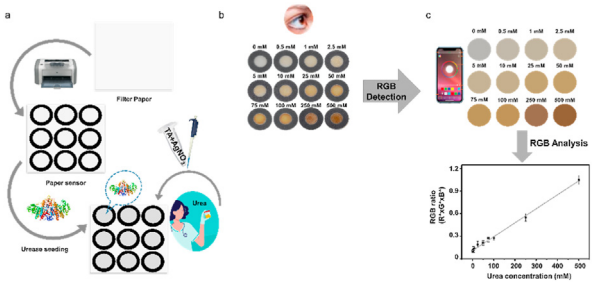

ARTICLE INFO

Article history:
Received 28 March 2021
Received in revised form
27 April 2021
Accepted 7 May 2021
Available online 19 May 2021

Keywords:
Urea
Urease
Colorimetric
Point-of-care bioassay
Smartphone-assisted biosensor

ABSTRACT

Smartphone-assisted point-of-care (POC) bioassay has brought a giant leap in personal healthcare system and environmental monitoring advancements. In this study, we developed a rapid and reliable colorimetric urea biosensor assisted by a smartphone. We employed hydrolysis of urea into NH_3 by urease, which activates the reduction power of tannic acid, to generate silver nanoparticles for a dramatic colorimetric response. The proposed urea biosensor was validated in a solution to provide high selectivity against various interferents in human urine. It had high sensitivity, with a limit of detection as low as 0.0036 mM, and a high reliability of 99% ± 2.9% via the standard addition method. The urea biosensor was successfully implanted on a paper to facilitate smartphone-assisted POC readout with a limit of detection of 0.58 mM and wide detection range of 500 mM, whereby direct diagnosis of human urine without dilution was realized. Our smartphone-assisted POC colorimetric urea biosensor will pave the way for daily monitoring systems of renal and hepatic dysfunction diseases.

1. Introduction

Smartphone-assisted point-of-care (POC) biosensors have garnered much attention because they provide a rapid and on-site diagnosis tool for daily healthcare systems without complicated instrumentation or high-standard expertise, saving labor, cost, and

* Corresponding author. School of Chemical Engineering, Sungkyunkwan University (SKKU), Suwon 16419, Republic of Korea.
E-mail address: dhkim1@skku.edu (D.-H. Kim).
[1] These authors contributed equally to this work.

https://doi.org/10.1016/j.aca.2021.338630
0003-2670/

treatment time for a wide range of diseases [1–3]. Urea is one of the most important biomolecular targets of POC biosensors [4] because it is the main product of nitrogen-based metabolism, mainly secreted from the human kidneys and liver [5–7]; thus, it provides pathophysiological information on renal and hepatic disorders [8–10]. Although urea exists in various body fluids, such as urine, saliva, and blood, the blood–urea–nitrogen test is the gold standard for urea bioassay [11]. Urine is the preferred fluid for POC diagnosis because the concentration of urea in urine is much higher (275–409 mM) than that in other body fluids (e.g., 2.5–7.14 mM in blood) [12], which facilitates tiny-volume diagnosis. It also has the most simple and noninvasive collection protocol compared with that of blood and saliva. Until now, various sensing strategies for quantitative urea analysis have been demonstrated by capillary electrophoresis [13,14], ELISA [15], and electrochemical methods [11,16–19]. However, these are time-consuming and require complex pretreatment, making urea bioassay unsuitable for POC diagnosis with urine.

To realize a POC biosensor, colorimetric detection of biomolecules is of great interest because it provides simpler detection mechanisms, real-time responses, and more intuitive readouts compared with methods such as electrochemistry, fluorophotometry, electrophoresis, chromatography, and spectrometry, which typically require complicated instrumentation, time-consuming processes, and expensive setups [20–25]. As colorimetric sensing units, plasmonic metal nanomaterials have been intensively studied because of their distinctive colorimetric responses in the presence of biomolecular targets, e.g., glucose [26], Hg^{2+} [27], cysteine [28], prostate-specific antigen [29], and cholesterol [30]. Despite the high potential of colorimetric detection, however, the development of POC biosensors based on plasmonic metal nanomaterials has remained largely unexplored, especially for smartphone-assisted urea bioassay.

Here, we demonstrate a highly sensitive colorimetric urea biosensor based on the generation of silver nanoparticles (AgNPs) through image analysis using a smartphone. We employ urease to hydrolyze urea into NH_3 and CO_2, which activates pH-responsive tannic acid to reduce Ag^+ ions into AgNPs. The amount of AgNPs is indicated by yellow color generation in the sensor units. We also demonstrate that the hydrolysis of urea is selectively triggered by urease, resulting in the colorimetric response of the sensing units with a linear function of the urea concentration. The developed urea biosensor shows a limit of detection (LOD) of 0.0036 mM, the lowest compared with that of previously reported colorimetric biosensors, which is important for tiny-volume diagnosis. We then implant the developed urea biosensor into a paper substrate and analyze the concentration of urea in human urine using a smartphone. Our smartphone-assisted urea biosensor has an LOD as low as 0.58 mM and a detection range as wide as 500 mM, which facilitates urea bioassay in human urine without any pretreatment (including dilution), proving its feasibility for daily POC diagnosis of renal and hepatic dysfunction diseases.

2. Materials and methods

2.1. Materials

Tannic acid (TA), silver nitrate ($AgNO_3$), urea (CH_4N_2O), sodium nitrate ($NaNO_3$), magnesium sulfate ($MgSO_4$), iron(III) chloride ($FeCl_3$), potassium phosphate PB (KH_2PO_4), iron(II) sulfate heptahydrate ($FeSO_4.7H_2O$), calcium nitrate ($Ca(NO_3)_2$), D-glucose, uric acid, creatinine, acetylcholine, glycine, L-alanine, L-phenylalanine, bovine serum albumin (BSA), cysteamine, urease enzyme (*Canavalia ensiformis* [Jack bean]) were purchased from Sigma Aldrich (South Korea) and used without further pretreatment purification. Deionized water filtered to 18 MΩ cm was used in all experiments.

2.2. Apparatus

The morphology of the prepared AgNPs was examined using transmission electron microscopy (JEM-2100F, JEOL) and scanning electron microscopy (SEM) (JSM7600F JEOL) at accelerating voltages of 15 kV. A Zetasizer (Nano-zs90, Malvern) was used to examine the size distribution of the synthesized nanoparticles based on dynamic light scattering (DLS). The absorbances of the prepared nanoparticles were monitored by UV–Vis spectroscopy (V 770, JASCO).

2.3. Validation of the effect of NH_3 on the generation of AgNPs

Urea is selectivity hydrolyzed into NH_3 and CO_2 under the catalytic activity of urease enzyme; NH_3 changes the solution pH, and TA reduces Ag^+ ions into AgNPs under basic conditions. To examine the effect of NH_3 on our urea sensing strategy, we tested the colorimetric responses of our sensor using an NH_3 standard solution. Here, 100 μL of $AgNO_3$ solution (15 mM) and 800 μL of aqueous TA solution (0.01 mg/mL) were mixed, and 100 μL of phosphate buffer (PB, 0.5 mM) with various NH_3 concentrations was added, followed by incubation for 20 min. The effect of NH_3 on our sensor was examined by measuring the change in absorption intensity around $\lambda = 413$ nm (corresponding to the generation of AgNPs) using the UV–Vis spectrometer.

2.4. Urea detection

A total of 50 μL of urease (10 U/mL) in 0.5 mM of PB solution was mixed with 50 μL of aqueous urea solutions of various concentrations and incubated for 10 min at 37 ± 1 °C in a water bath. Subsequently, the sensing solution, consisting of 800 μL of TA (0.01 mg/mL) and 100 μL of $AgNO_3$ (15 mM), was added and incubated for 20 min. The urea concentration was examined by measuring the change in absorption intensity around $\lambda = 413$ nm using the UV–Vis spectrometer.

2.5. Selectivity test

The selectivity of the developed urea biosensor was investigated against various inorganic salts, including sodium nitrate, magnesium sulfate, iron(III) chloride, iron(II) sulfate heptahydrate, potassium phosphate, and calcium nitrate, as well as several species with similar structures to urea that are present in human urine, such as uric acid, creatinine, glucose, acetylcholine, glycine, L-alanine, L-phenylalanine, BSA, and cysteamine, following the same procedure as the urea assay. The concentration of all interferents was 1 mM, except for BSA and cysteamine at 0.1 mM.

2.6. The detection of urea in human urine

The feasibility of the developed urea biosensor was validated using two human urine samples collected from two middle-aged adult males. The urine samples were diluted 400 times before the urea bioassay. The urea concentration in the urine samples was determined using the standard addition method. First 50 μL of the urine sample (unknown urea concentration and called as zero spiked sample) was incubated with a 50 μL of urease for 10 min, followed by detecting the signal as described in section 2.4. Second, different concentrations of standard urea were in spiked in the urine sample and the signal was detected as described in the first step. Finally, a relationship between the spiked urea concentration (X-axis) and the change in the absorption intensity (Y-axis) was

provided for estimating the concentration unknown urea in the urine sample (The intersection of the straight line with X-axis refer to the unknown urea concentration in the urine sample). The recovery rate (%) was calculated according to the following equation:

$$\text{Recovery rate}(\%) = \frac{\text{Measured concentration}}{\text{Added concentration}} \times 100$$

2.7. Smartphone-assisted urea biosensor

A paper sheet for the smartphone-assisted urea biosensor was fabricated according to previously published work [31]. Using a laser printer, we printed a hydrophobic black zone (waxy ink) around a hydrophilic sampling zone (filter paper, Whatman). After fabricating the paper, 50 μL of urease (20 U/mL, 0.5 mM PB solution) was loaded on the sampling hydrophilic zone; then, 50 μL of urea at various concentrations was added and kept for 10 min to induce the reaction between urea and urease. Then, 50 μL of the sensing solution consisting of TA (0.05 mg/mL, 800 μL) and $AgNO_3$ (100 mM, 100 μL) was added on the hydrophilic sampling zone and kept for 10 min before analysis using a smartphone's RGB software. After evaluating the performance of the urea biosensor, we examined the concentration of urea in human urine after its dilution 100 times.

3. Results and discussion

3.1. Optimization of the colorimetric urea biosensor using NH_3

The mechanism of our urea biosensor is depicted in Scheme 1. Urea is decomposed into NH_3 and CO_2 by urease to increase the system pH, resulting in the reduction of Ag^+ ions into AgNPs by TA, which consists of glucose as a central core linked with polygalloyl ester chains to serves as a reducing agent under alkaline conditions [32–35]. As the system pH increases via urea hydrolysis, a higher reduction efficiency of TA is attained to generate more AgNPs for larger colorimetric responses (Scheme 1).

As shown in Fig. 1a (red line), in our experiment, the addition of urea (target) and urease (enzyme) into the solution containing both $AgNO_3$ and TA (sensing solution) leads to the appearance of an absorption band at around 413 nm, confirming the generation of AgNPs (red line). The formation of AgNPs was also confirmed by TEM (Fig. 1b). The sensing solution alone did not trigger the generation of the AgNPs, nor did the addition of either urea or urease individually into the sensing solution. As confirmed by UV–Vis (Fig. 1a, blue line) and TEM (Fig. 1c), the addition of NH_3 to the sensing solution is what led to the AgNP generation.

As the reduction power of TA is pH-dependent, both the TA concentration and solution pH had an effect on the sensitivity of the colorimetric sensor. To find the optimal working condition of the colorimetric sensor, TA of various concentrations, ranging from 0.005 to 0.05 mg/mL (800 μL), was examined by NH_3 (0.2–2 mM, 100 μL) with a fixed concentration of $AgNO_3$ (10 mM, 100 μL) (Fig. 1d). From the TA titration, two different trends dependent on the TA concentration were observed. At high concentrations of NH_3 (>1 mM), TA induced an absorption intensity increase at 413 nm. On the contrary, at low NH_3 concentrations (<0.4 mM), TA at high concentrations (>0.025 mg/mL) caused the absorption intensity to decrease from its peak at 413 nm. This was because at high concentrations, TA consumed NH_3 to lower the solution pH, hindering the generation of AgNPs. Based on this finding, 0.01 mg/mL of TA was selected as the optimum concentration, ensuring that the colorimetric sensor covers the detection range from low to high urea concentrations. Next, because the concentration of $AgNO_3$ also has an essential role in the reduction process of Ag^+ ions, $AgNO_3$ at various concentrations, from 10 to 20 mM, was tested with the

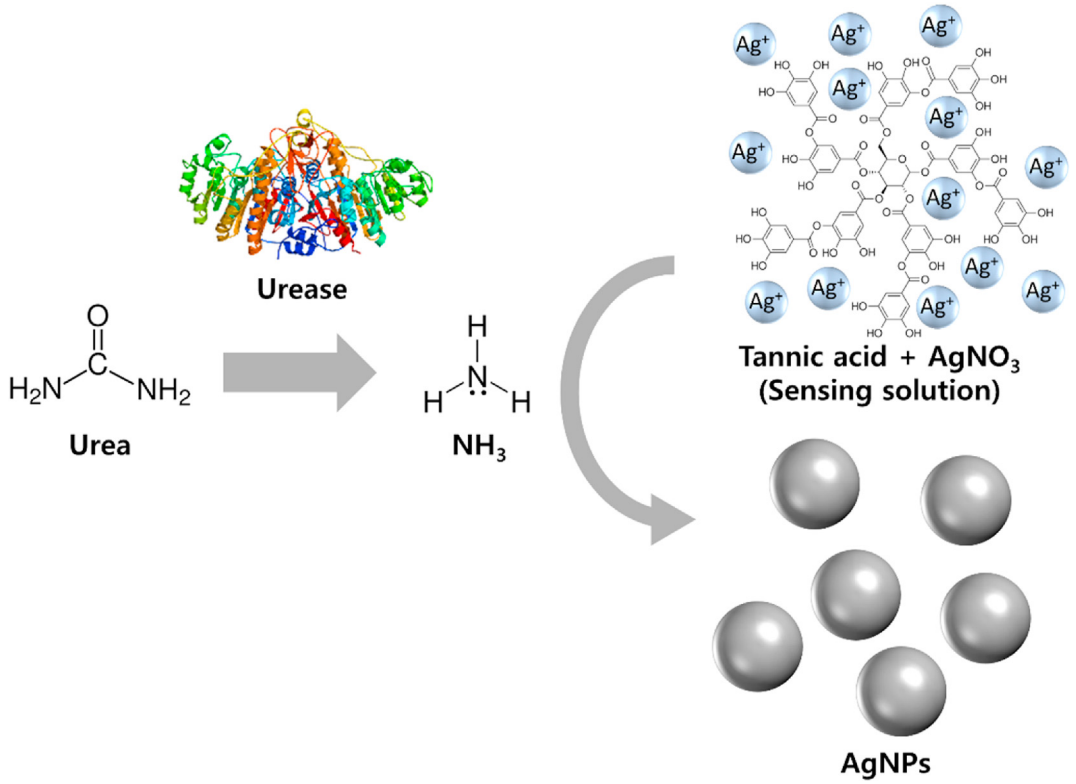

Scheme 1. The mechanism of the colorimetric urea biosensor based on the generation of AgNPs as a function of the pH-responsive reduction of Ag^+ ions by TA.

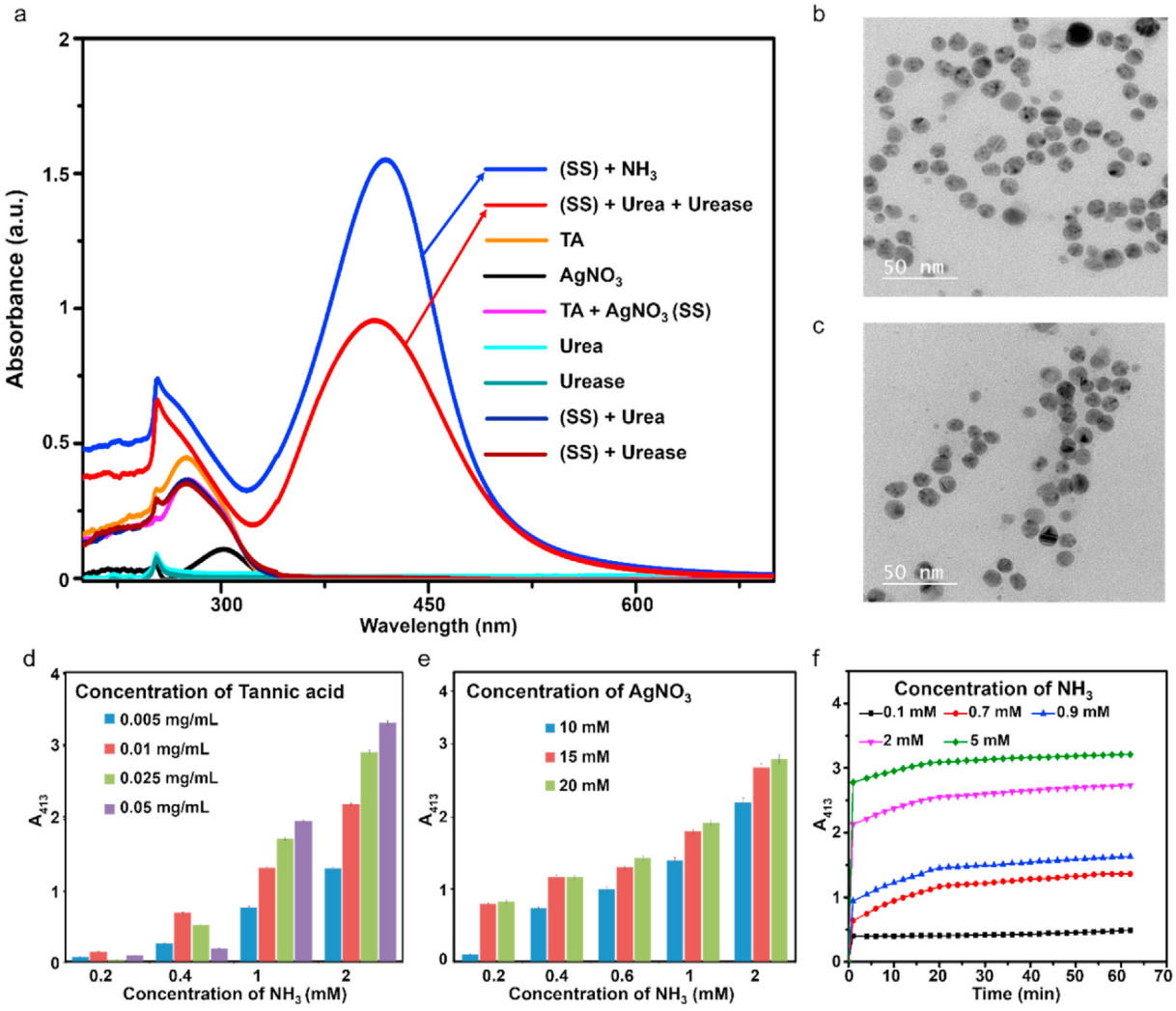

Fig. 1. (**a**) UV–Vis absorbance of reagents, demonstrating the feasibility of the sensing mechanism. (**b**–**c**) TEM of AgNPs in the presence of (**b**) both urea (1 mM, 50 μL) and urease (10 U/mL, 50 μL) and (**c**) NH_3 (1 mM, 100 μL). In **b** and **c**, the concentrations of $AgNO_3$ and TA were 15 mM and 0.01 mg/mL, respectively. (**d**) UV–Vis absorbance at various TA concentrations as a function of NH_3 concentration; the concentration of $AgNO_3$ was fixed at 10 mM. (**e**) UV–Vis absorbance at various $AgNO_3$ concentrations as a function of NH_3 concentration; the concentration of TA was fixed at 0.01 mg/mL (**f**) UV–Vis absorbance of various concentrations of NH_3 as a function of reaction time; the concentrations of TA and $AgNO_3$ were fixed at 0.01 mg/mL and 15 mM, respectively.

optimized TA concentration of 0.01 mg/mL (Fig. 1e). Based on the $AgNO_3$ optimization, 15 mM of $AgNO_3$ was selected as the optimum concentration because both 15 and 20 mM of $AgNO_3$ triggered a similar absorption intensity and 10 mM of $AgNO_3$ showed a relatively low absorbance. Finally, to find the optimal reaction time, the peak intensity was monitored after adding NH_3 at the optimized TA (0.01 mg/mL) and $AgNO_3$ (15 mM) concentrations. A reaction time of 20 min was selected as the optimal time since saturation of the reaction was observed after 20 min (Fig. 1f). Under these optimized conditions, the colorimetric sensor was tested with NH_3 of various concentrations (Fig. S1), and we confirmed the continuous and smooth increase of the absorption intensity at 413 nm, which corresponded to the increased amount of AgNPs.

3.2. Urea detection

After the TA, $AgNO_3$, and incubation time optimization, the reaction between urea and urease was optimized to achieve the highest NH_3 release; the optimal condition for the urease concentration and incubation time was 10 U/mL (Fig. S2). The validity of the developed urea biosensor is shown in Fig. 2. As the urea concentration increased, the absorption intensity at 413 nm increased because of the generation of AgNPs (Fig. 2a), and the distinctive color changed from colorless to yellow and brown (Fig. 2a inset). The developed urea biosensor exhibited a quantitatively linear trend from 0.00625 to 1 mM (Fig. 2b inset) with an LOD of 0.0036 mM according to equation $3\sigma/m$, where m is the calibration curve slope and σ is the standard deviation of blank. The obtained LOD of our colorimetric sensor showed the best sensitivity among previously reported colorimetric urea biosensors and was comparable to the lowest LOD of urea detection ever demonstrated by electrochemical methods, as summarized in Table 1.

Fig. 3 shows the SEM images of the generated AgNPs, dependent on the various urea concentrations. As the urea concentration increased, the amount of generated AgNPs increased with decreasing particle sizes. This agreed with the increased absorption intensity with a slight blue shift observed in Fig. 2a and the DLS measurements (Fig. S3). A mild reducing agent triggered slow nucleation of the AgNPs and produced larger particle sizes, whereas a strong reducing agent accelerated the nucleation of the AgNPs,

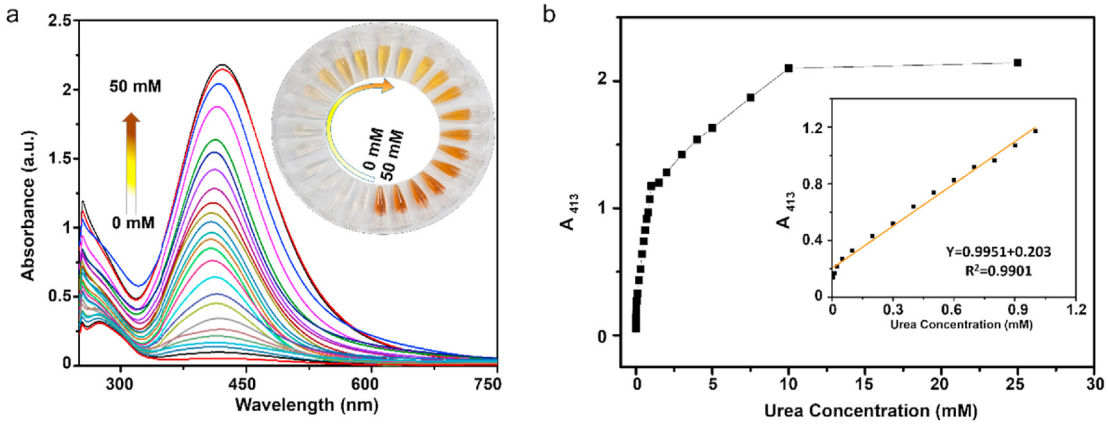

Fig. 2. (a) UV–Vis spectra of the developed colorimetric urea biosensor and corresponding color image (inset). (b) Absorption intensity at 413 nm as a function of urea concentrations from 0 to 25 mM, with a linear calibration curve from 0.00625 to 1 mM (inset). (For interpretation of the references to color in this figure legend, the reader is referred to the Web version of this article.)

Table 1
Comparison with previously reported urea biosensors.

Methods	Range (mM)	LOD (mM)	Response time (min)	Ref.
Electro-chemical	0.000066–20.6	0.000047	2	[36]
	1–8	0.14	2	[37]
	0.05–2.5	0.02	–	[38]
	0.002–0.08	0.001	2	[19]
	0.02–0.8	0.02	–	[39]
	0.5–68	0.5	2	[40]
	0.2–100	0.2	–	[41]
	0.83–16.65	–	2	[42]
Fluorometric	0.057–13	0.01	31	[43]
	0.25–5	0.01	45	[44]
	0.2–6	0.2	31	[45]
	0.05–3	0.02	40	[46]
	0.014–60	0.014	40	[47]
	10–100	0.027	4.8	[48]
	0.01–120	0.01	10	[49]
	0.055–0.55	0.055	40	[50]
Colorimetric	20–150	20	40	[51]
	0–10	0.01	35	[52]
	0.02–0.4	0.005	40	[7]
	0.00625–1	0.0036	30	Our work

resulting in a small particle size because of the rapid depletion of Ag^+ ions [53,54]. For large colorimetric responses, a high urea concentration is preferred since the absorption efficiency of plasmonic nanoparticles is higher when the particle size is smaller and a larger amount of plasmonic nanoparticles leads to strong absorption [53,54].

The selectivity of the developed colorimetric urea biosensor was investigated using substances with similar chemical structures to urea, including uric acid, creatinine, glucose, acetylcholine, glycine, L-alanine, L-phenylalanine, BSA, cysteamine, and various salts present in urine that may interfere with urine detection. The developed colorimetric sensor was confirmed to be highly selective by the observed absorption intensity at 413 nm (Fig. 4) and distinguishable yellow color (Fig. 4 inset image) because urease does not exist in human urine.

3.3. The detection of urea in human urine

Two human urine samples collected from volunteers were used to examine the applicability of the developed urea biosensor for POC diagnosis. The standard addition method was used for determining the concentration of urea in the samples. The urine samples were diluted 400 times before the measurements to match the detection range of our developed sensor (0.00625–1 mM). Firstly, the signal of the urine sample (zero spiked sample) was recorded as described in section 2.6, then various concentrations of standard urea of was added, after which the absorption intensity at 413 nm as a function of the added standard urea was measured, as shown in Fig. 5a and b. The two urine samples showed linear relationships between the absorption intensity at 413 nm and concentration of added urea in the urine samples, with a visual colorimetric response (Fig. 5c and d). The intersection at the Y-axis, which referred to the initial concentration of urea in the urine samples (zero spiked sample), was found to equal 214.6 and 69.86 mM (Table 2). To examine the sensor validity, a recovery test was performed. The high recovery rates in Table 2 clarify that the developed urea biosensor has high selectivity, sensitivity, and reliability.

3.4. Smartphone-assisted POC colorimetric urea biosensor

The paper substrate for the urea biosensor was fabricated as outlined in Fig. 6a using a hydrophilic sample zone surrounded by a hydrophobic printed wall. The urease was immobilized on the hydrophilic zone with urea solutions of various concentrations

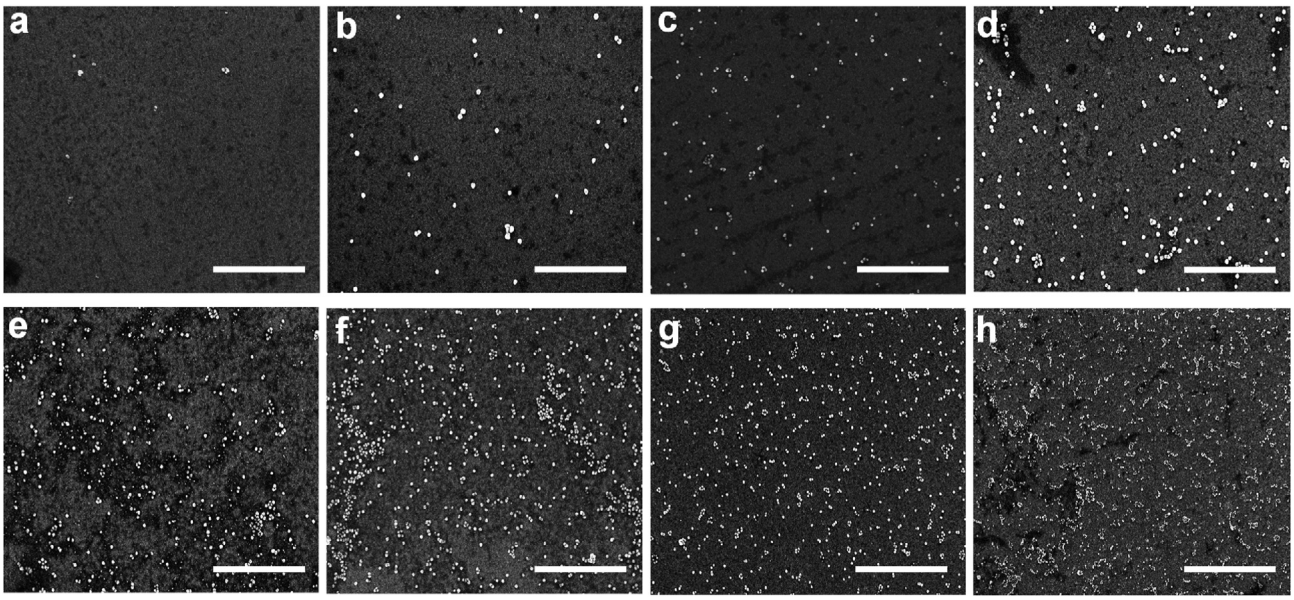

Fig. 3. (a–f) SEM images of the AgNPs as a function of urea concentrations. The urea concentrations were 0.0 (a), 0.2 (b), 0.3 (c), 0.4 (d), 0.7 (e), 0.8 (f), 1 (g), and 10 (h) mM, while the urease, TA, and $AgNO_3$ concentrations were fixed at 10 U/mL, 0.01 mg/mL, and 15 mM, respectively. Scale bar is 500 nm.

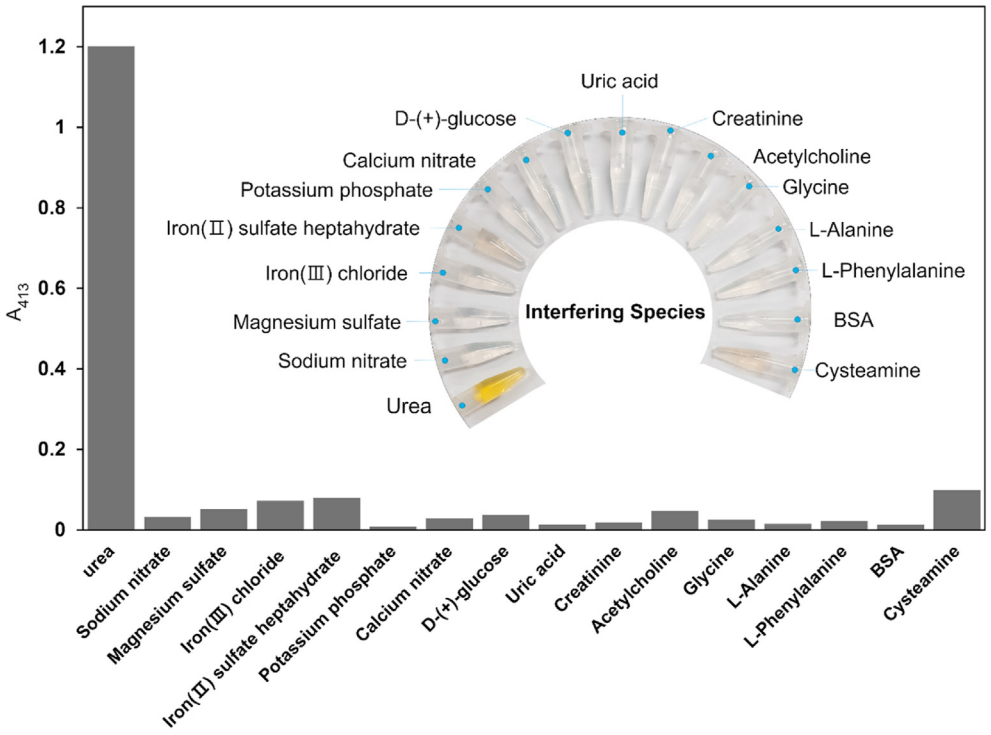

Fig. 4. Selectivity of the developed colorimetric urea biosensor against several interferents (inset image represents the colorimetric responses to the interferents).

(0–500 mM). Then, the sensing solution consisting of TA and $AgNO_3$ was subsequently added to the hydrophilic zone. The paper sensor was able to roughly detect the urea concentrations by a color tractable by the naked eye (Fig. 6b**).** A smartphone camera was used to obtain more precise color information on the paper urea biosensor, following the literature [55–57]. The RGB values were obtained from the sensing units after dropping the sensing solution containing various urea concentrations and analyzed to attain a linear relationship based on the urea concentrations.

Different RGB ratios as functions of urea concentrations have been conducted, such as direct color intensity (R, G, or B), R/G ratio, and R/B ratio as functions of urea concentration. However, the linear response R^2 was poor in case of direct color intensity and in case of the R/G or R/B ratios it produced good R^2 (0.94–0.96) with a dynamic range of 5–250 mM (data not shown). Some published work conducted a correction factor for the RGB values by removing color contrasting between the sample with and without targets [56]; therefore, we adapted a mathematic model to measure the

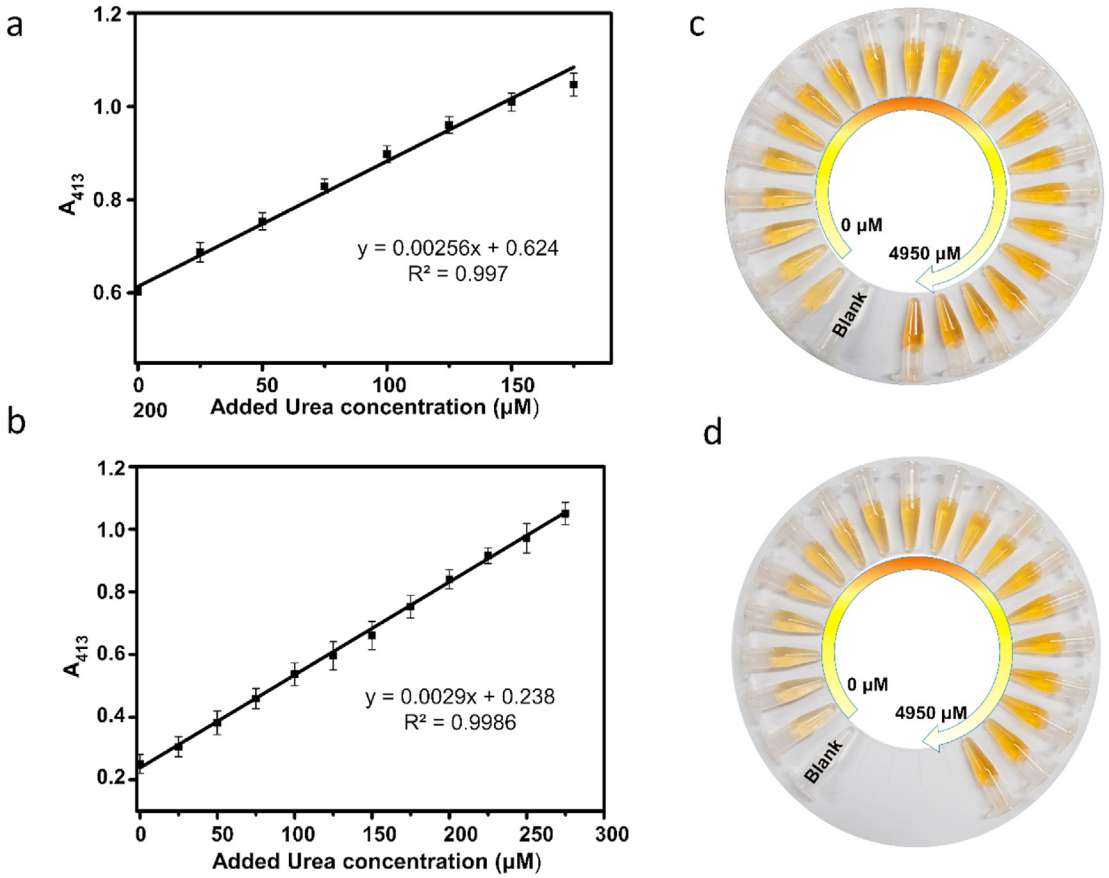

Fig. 5. (a–b) Linear standard calibration curve using the absorption intensity at 413 nm as a function of added urea concentration compared with zero-added-urine sample 1 (a) and sample 2 (b). (c–d) Photo of the visual detection of urea in urine sample 1 (c) and sample 2 (d).

Table 2
Analytical results of urea detection in human urine.

Sample	Added (mM)	Found (mM)	Recoveries (%)	RSD (%, n = 3)
Human Urine 1	0	214.6	–	0.6
	44	257.5	97.4	3.4
	88	300.92	98.1	2.4
	132	350.8	103.2	2.6
Human Urine 2	0	69.86	–	2.3
	44	114.6	101.7	1.7
	88	156.35	98.3	1.4
	132	195.66	95.3	2.9

RGB ratios with a correction factor for improving the response sensitivity (as outlined inEquation (4), following Equation (1)–3) by considering the correction of the RGB values via contrasting the color removal between the samples with and without the target [56],

$$R^* = \frac{(R_0 - R_H)}{(R_C)} \quad (1)$$

$$G^* = \frac{(G_0 - G_H)}{(G_C)} \quad (2)$$

$$B^* = \frac{(B_0 - B_H)}{(B_C)} \quad (3)$$

$$RGB\ \ ratio = R^* \times G^* \times B^* \quad (4)$$

The corrected red (R^*), green (G^*), and blue (B^*) color intensity was calculated followingEquations (1)–(3), respectively, where the R_o is the red color intensity in presence of zero urea, R_H is the red color intensity in the presence of the highest urea concentration tested, whereas R_C is the red color intensity in the presence of specified urea concentrations. Similarly, the G^* and B^* was calculated based on their intensity variations with urea concentrations, as mentioned in the R^*.

The obtained corrected RGB ratio showed a good linear correlation with the urea concentrations, and the linear regression R^2 values were as high as 0.99. The dynamic linear detection range was sufficiently wide, ranging from 0 to 500 mM according to the following equation: $y = 0.001x + 0.109$ ($R^2 = 0.993$), where y is the RGB and x is the urea concentration (Fig. 6c). The LOD was calculated to be considerably low at 0.58 mM according to the following equation: $3\sigma/m$.

Then, we validated the smartphone-assisted POC colorimetric urea biosensor using human urine sample 1 after diluting 100 times, which had been previously analyzed by the solution system ([Fig. 5a–b]) based on RGB extraction using the provided equation: $y = 0.001x + 0.109$, where y was calculated based on Equation (1–4). The determined urea in human urine sample 1 was 216.8 mM (Fig. 7), which matched with that obtained by the solution system (Table 1). This result demonstrated that the developed smartphone-assisted POC colorimetric urea biosensor is highly feasible and applicable to visual and quantitative urea bioassay for POC diagnosis.

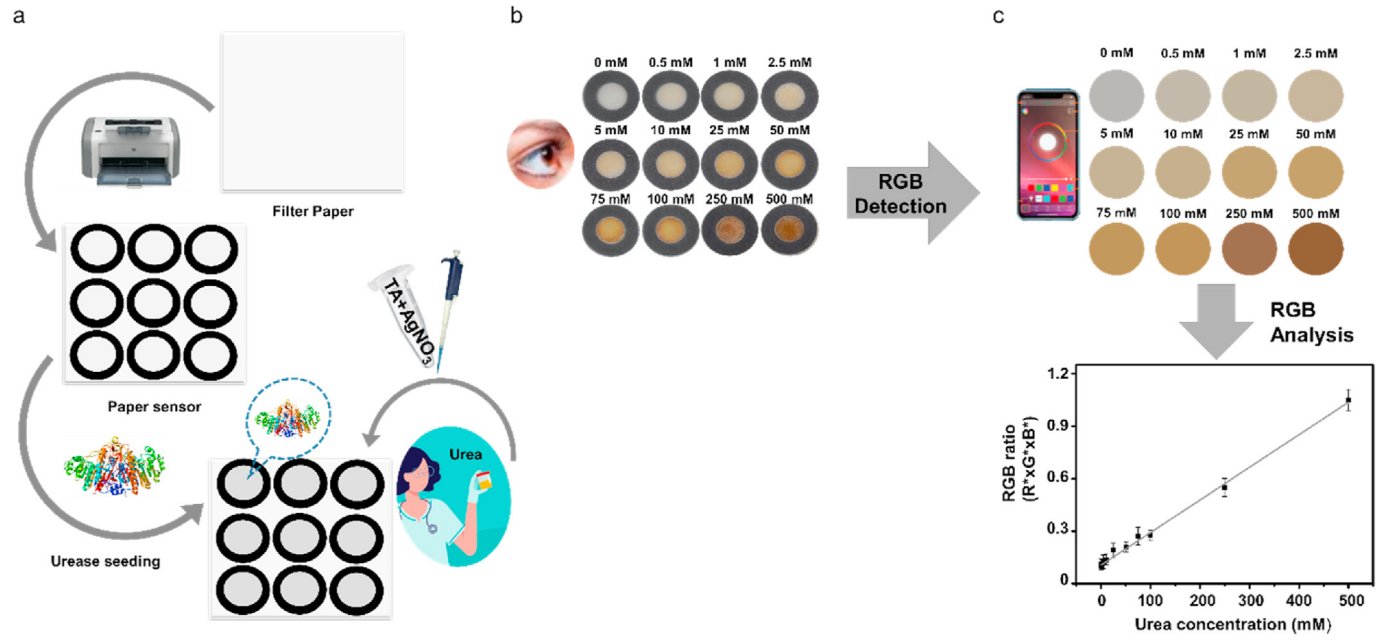

Fig. 6. (**a**) Schematic illustration of smartphone-assisted POC colorimetric urea biosensor. (**b**–**c**) Analytical colorimetric responses to urea concentrations by the naked eye (**b**) and smartphone-assisted RGB ratios (**c**).

			
R value	180	179	178
G value	169	170	169
B value	139	139	141
R*×G*×B*	0.116391	0.116754	0.116716
Calculate concentration of urine, 100time dilute (Y=0.0019X+0.1125)	2.047	2.238	2.218
Final concentration of urine(mM)	204.7	223.8	221.8
Average(mM)		216.8	

Fig. 7. The data extracted from human urine sample 1 using the smartphone-assisted POC colorimetric urea biosensor.

4. Conclusions

We developed a smartphone-assisted POC colorimetric urea biosensor by employing hydrolysis of urea into NH_3 via urease to activate the reduction power of TA for the generation of AgNPs, which are responsible for the dramatic colorimetric response. The developed urea biosensor has high selectivity toward various interferents in human urine, high sensitivity (with a considerably low LOD at 0.58 mM), and a wide detection range of 500 mM, resulting in direct diagnosis of human urine without dilution. Our smartphone-assisted POC colorimetric urea biosensor could pave the way for daily monitoring systems of renal and hepatic

dysfunction diseases.

CRediT authorship contribution statement

Cheol-Kyun Choi: performed most of the experiments, including sample preparation and optical characterizations. All authors analyzed the data and wrote and revised the manuscript. **Samy M. Shaban:** performed most of the experiments, including sample preparation and optical characterizations. All authors analyzed the data and wrote and revised the manuscript. **Byeong-Seok Moon:** conceived and supervised the project, All authors analyzed the data and wrote and revised the manuscript. **Do-Gi Pyun:** conceived and supervised the project, All authors analyzed the data and wrote and revised the manuscript. **Dong-Hwan Kim:** conceived and supervised the project, All authors analyzed the data and wrote and revised the manuscript.

Declaration of competing interest

The authors declare that they have no known competing financial interests or personal relationships that could have appeared to influence the work reported in this paper.

Acknowledgments

This work was supported by the National Research Foundation of Korea (NRF) grant funded by the Korea government (MSIT) (2020R1A5A1018052) and Basic Science Research Program through the National Research Foundation of Korea (NRF) funded by the Ministry of Education (NRF-2019R1A2C2085177). This research was also supported by Korea Basic Science Institute (National research Facilities and Equipment Center) grant funded by the Ministry of Education (grant No. 2020R1A6C101A191).

Appendix A. Supplementary data

Supplementary data to this article can be found online at https://doi.org/10.1016/j.aca.2021.338630.

References

[1] X. Kou, L. Tong, Y. Shen, W. Zhu, L. Yin, S. Huang, F. Zhu, G. Chen, G. Ouyang, Smartphone-assisted robust enzymes@MOFs-based paper biosensor for point-of-care detection, Biosens. Bioelectron. 156 (2020) 112095.
[2] Y. Xing, Q. Zhu, X. Zhou, P. Qi, A dual-functional smartphone-based sensor for colorimetric and chemiluminescent detection: a case study for fluoride concentration mapping, Sensor. Actuator. B Chem. (2020) 319.
[3] W. Zhao, S. Tian, L. Huang, K. Liu, L. Dong, J. Guo, A smartphone-based biomedical sensory system, Analyst 145 (8) (2020) 2873–2891.
[4] A. Soni, R.K. Surana, S.K. Jha, Smartphone based optical biosensor for the detection of urea in saliva, Sensor. Actuator. B Chem. 269 (2018) 346–353.
[5] F. Kuralay, H. Özyörük, A. Yıldız, Potentiometric enzyme electrode for urea determination using immobilized urease in poly(vinylferrocenium) film, Sensor. Actuator. B Chem. 109 (2) (2005) 194–199.
[6] M. Gutiérrez, S. Alegret, M. del Valle, Potentiometric bioelectronic tongue for the analysis of urea and alkaline ions in clinical samples, Biosens. Bioelectron. 22 (9) (2007) 2171–2178.
[7] H.-H. Deng, G.-L. Hong, F.-L. Lin, A.-L. Liu, X.-H. Xia, W. Chen, Colorimetric detection of urea, urease, and urease inhibitor based on the peroxidase-like activity of gold nanoparticles, Anal. Chim. Acta 915 (2016) 74–80.
[8] V. Jha, G. Garcia-Garcia, K. Iseki, Z. Li, S. Naicker, B. Plattner, R. Saran, A.Y.-M. Wang, C.-W. Yang, Chronic kidney disease: global dimension and perspectives, Lancet 382 (9888) (2013) 260–272.
[9] W.G. Couser, G. Remuzzi, S. Mendis, M. Tonelli, The contribution of chronic kidney disease to the global burden of major noncommunicable diseases, Kidney Int. 80 (12) (2011) 1258–1270.
[10] A.J. Taylor, P. Vadgama, Analytical reviews in clinical biochemistry: the estimation of urea, Ann. Clin. Biochem. 29 (3) (1992) 245–264.
[11] K.-H. Wang, J.-C. Hsieh, C.-C. Chen, H.-W. Zan, H.-F. Meng, S.-Y. Kuo, M.T.N. Nguyễn, A low-cost, portable and easy-operated salivary urea sensor for point-of-care application, Biosens. Bioelectron. 132 (2019) 352–359.
[12] L. Liu, H. Mo, S. Wei, D. Raftery, Quantitative analysis of urea in human urine and serum by 1H nuclear magnetic resonance, Analyst 137 (3) (2012) 595–600.
[13] X. Liu, J. Yang, S. Sun, L. Guo, L. Yang, Enzyme and inhibition assay of urease by continuous monitoring of the ammonium formation based on capillary electrophoresis, Electrophoresis 37 (20) (2016) 2692–2698.
[14] C.-P. Witte, N. Medina-Escobar, In-gel detection of urease with nitroblue tetrazolium and quantification of the enzyme from different crop plants using the indophenol reaction, Anal. Biochem. 290 (1) (2001) 102–107.
[15] B.E. Patten, P.A. Higgins, K.G. Whithear, A urease-ELISA for the detection of mycoplasma infections in poultry, Aust. Vet. J. 61 (5) (1984) 151–155.
[16] W.-J.L. Ma, , C.-H., J.-L. Lin, S.-H. Chou, P.-H. Chen, M.-J. Syu, S.-H. Kuo, S.-C. Lai, A portable low-power acquisition system with a urease bioelectrochemical sensor for potentiometric detection of urea concentrations, Sensors 16 (2016) 474–487.
[17] J.H.J. Hubalek, V. Adam, O. Krystofova, D. Huska, M. Masarik, L. Trnkova, A. Horna, K. Klosova, M. Adamek, J. Zehnalek, R. Kizek, Spectrometric and voltammetric analysis of urease – nickel nanoelectrode as an electrochemical sensor, Sensors 7 (2007) 1238–1255.
[18] E. Prats-Alfonso, L. Abad, N. Casañ-Pastor, J. Gonzalo-Ruiz, E. Baldrich, Iridium oxide pH sensor for biomedical applications. Case urea–urease in real urine samples, Biosens. Bioelectron. 39 (1) (2013) 163–169.
[19] S. Jakhar, C.S. Pundir, Preparation, characterization and application of urease nanoparticles for construction of an improved potentiometric urea biosensor, Biosens. Bioelectron. 100 (2018) 242–250.
[20] M.S. Bloomfield, A sensitive and rapid assay for 4-aminophenol in paracetamol drug and tablet formulation, by flow injection analysis with spectrophotometric detection, Talanta 58 (6) (2002) 1301–1310.
[21] H. Filik, M. Hayvalı, E. Kılıç, R. Apak, D. Aksu, Z. Yanaz, T. Çengel, Development of an optical fibre reflectance sensor for p-aminophenol detection based on immobilised bis-8-hydroxyquinoline, Talanta 77 (1) (2008) 103–109.
[22] L. Monser, F. Darghouth, Simultaneous LC determination of paracetamol and related compounds in pharmaceutical formulations using a carbon-based column, J. Pharmaceut. Biomed. Anal. 27 (6) (2002) 851–860.
[23] F.A. Mohamed, M.A. AbdAllah, S.M. Shammat, Selective spectrophotometric determination of p-aminophenol and acetaminophen, Talanta 44 (1) (1997) 61–68.
[24] E. Wyszecka-Kaszuba, M. Warowna-Grześkiewicz, Z. Fijałek, Determination of 4-aminophenol impurities in multicomponent analgesic preparations by HPLC with amperometric detection, J. Pharmaceut. Biomed. Anal. 32 (4) (2003) 1081–1086.
[25] Q. Chu, L. Jiang, X. Tian, J. Ye, Rapid determination of acetaminophen and p-aminophenol in pharmaceutical formulations using miniaturized capillary electrophoresis with amperometric detection, Anal. Chim. Acta 606 (2) (2008) 246–251.
[26] S. Basiri, A. Mehdinia, A. Jabbari, A sensitive triple colorimetric sensor based on plasmonic response quenching of green synthesized silver nanoparticles for determination of Fe2+, hydrogen peroxide, and glucose, Colloid. Surface. Physicochem. Eng. Aspect. 545 (2018) 138–146.
[27] F. Faghiri, F. Ghorbani, Colorimetric and naked eye detection of trace Hg2+ ions in the environmental water samples based on plasmonic response of sodium alginate impregnated by silver nanoparticles, J. Hazard Mater. 374 (2019) 329–340.
[28] D. Rithesh Raj, C. Sudarsanakumar, Surface plasmon resonance based fiber optic sensor for the detection of cysteine using diosmin capped silver nanoparticles, Sensor Actuator Phys. 253 (2017) 41–48.
[29] J. Liang, C. Yao, X. Li, Z. Wu, C. Huang, Q. Fu, C. Lan, D. Cao, Y. Tang, Silver nanoprism etching-based plasmonic ELISA for the high sensitive detection of prostate-specific antigen, Biosens. Bioelectron. 69 (2015) 128–134.
[30] H.V. Tran, T.V. Nguyen, L.T.N. Nguyen, H.S. Hoang, C.D. Huynh, Silver nanoparticles as a bifunctional probe for label-free and reagentless colorimetric hydrogen peroxide chemosensor and cholesterol biosensor, J. Sci.: Advanced Materials and Devices 5 (3) (2020) 385–391.
[31] S.M. Shaban, J.Y. Lee, D.-H. Kim, Dual-surfactant-Capped Ag nanoparticles as a highly selective and sensitive colorimetric sensor for citrate detection, ACS Omega 5 (19) (2020) 10696–10703.
[32] K. Yoosaf, B.I. Ipe, C.H. Suresh, K.G. Thomas, In situ synthesis of metal nanoparticles and selective naked-eye detection of lead ions from aqueous media, J. Phys. Chem. C 111 (34) (2007) 12839–12847.
[33] Z. Yi, X. Li, X. Xu, B. Luo, J. Luo, W. Wu, Y. Yi, Y. Tang, Green, effective chemical route for the synthesis of silver nanoplates in tannic acid aqueous solution, Colloid. Surface. Physicochem. Eng. Aspect. 392 (1) (2011) 131–136.
[34] A.E. Hagerman, K.M. Riedl, G.A. Jones, K.N. Sovik, N.T. Ritchard, P.W. Hartzfeld, T.L. Riechel, High molecular weight plant polyphenolics (tannins) as biological antioxidants, J. Agric. Food Chem. 46 (5) (1998) 1887–1892.
[35] E. Bulut, M. Özacar, Rapid, facile synthesis of silver nanostructure using hydrolyzable tannin, Ind. Eng. Chem. Res. 48 (12) (2009) 5686–5690.
[36] T.H.V. Kumar, A.K. Sundramoorthy, Non-Enzymatic electrochemical detection of urea on silver nanoparticles anchored nitrogen-doped single-walled carbon nanotube modified electrode, J. Electrochem. Soc. 165 (8) (2018) B3006–B3016.
[37] J. Liu, R. Siavash Moakhar, A. Sudalaiyadum Perumal, H.N. Roman, S. Mahshid, S. Wachsmann-Hogiu, An AgNP-deposited commercial electrochemistry test strip as a platform for urea detection, Sci. Rep. 10 (1) (2020) 9527.
[38] S. Lu, Z. Gu, M. Hummel, Y. Zhou, K. Wang, B.B. Xu, Y. Wang, Y. Li, X. Qi, X. Liu, Nickel oxide immobilized on the carbonized eggshell membrane for

electrochemical detection of urea, J. Electrochem. Soc. 167 (10) (2020) 106509.
[39] I. Vostiar, J. Tkac, E. Sturdik, P. Gemeiner, Amperometric urea biosensor based on urease and electropolymerized toluidine blue dye as a pH-sensitive redox probe, Bioelectrochemistry 56 (1) (2002) 113–115.
[40] R. Singhal, A. Gambhir, M.K. Pandey, S. Annapoorni, B.D. Malhotra, Immobilization of urease on poly(N-vinyl carbazole)/stearic acid Langmuir–Blodgett films for application to urea biosensor, Biosens. Bioelectron. 17 (8) (2002) 697–703.
[41] A.S. Emami Meibodi, S. Haghjoo, Amperometric urea biosensor based on covalently immobilized urease on an electrochemically polymerized film of polyaniline containing MWCNTs, Synth. Met. 194 (2014) 1–6.
[42] M. Tyagi, M. Tomar, V. Gupta, Glad assisted synthesis of NiO nanorods for realization of enzymatic reagentless urea biosensor, Biosens. Bioelectron. 52 (2014) 196–201.
[43] Z. Li, Q. Zhang, H. Huang, C. Ren, S. Ouyang, Q. Zhao, L-noradrenaline functionalized near-infrared fluorescence CdSeTe probe for the determination of urea and bioimaging of HepG2 Cells, Talanta 171 (2017) 16–24.
[44] H.-H. Deng, K.-L. Li, Q.-Q. Zhuang, H.-P. Peng, Q.-Q. Zhuang, A.-L. Liu, X.-H. Xia, W. Chen, An ammonia-based etchant for attaining copper nanoclusters with green fluorescence emission, Nanoscale 10 (14) (2018) 6467–6473.
[45] S. Liu, F. Shi, L. Chen, X. Su, Dopamine functionalized CuInS2 quantum dots as a fluorescence probe for urea, Sensor. Actuator. B Chem. 191 (2014) 246–251.
[46] S. Pang, A pH sensitive fluorescent carbon dots for urea and urease detection, Fullerenes, Nanotub. Carbon Nanostruct. 28 (9) (2020) 752–760.
[47] L. Bi, X.-t. Dong, Y.-h. Yu, Room-temperature phosphorescence sensor based on manganese doped zinc sulfide quantum dots for detection of urea, J. Lumin. 153 (2014) 356–360.
[48] H. Dinh Duong, J. Il Rhee, Development of a ratiometric fluorescent urea biosensor based on the urease immobilized onto the oxazine 170 perchlorate-ethyl cellulose membrane, Talanta 134 (2015) 333–339.
[49] C.-P. Huang, Y.-K. Li, T.-M. Chen, A highly sensitive system for urea detection by using CdSe/ZnS core-shell quantum dots, Biosens. Bioelectron. 22 (8) (2007) 1835–1838.
[50] H.-H. Deng, G.-W. Wu, Z.-Q. Zou, H.-P. Peng, A.-L. Liu, X.-H. Lin, X.-H. Xia, W. Chen, pH-Sensitive gold nanoclusters: preparation and analytical applications for urea, urease, and urease inhibitor detection, Chem. Commun. 51 (37) (2015) 7847–7850.
[51] P. Kumar, P. Ramulu Lambadi, N. Kumar Navani, Non-enzymatic detection of urea using unmodified gold nanoparticles based aptasensor, Biosens. Bioelectron. 72 (2015) 340–347.
[52] Y. Wang, X. Luo, L. Zhang, S. Zhang, L. Zhang, A reversible, colorimetric, pH-responsive indole-based hydrogel and its application in urea detection, RSC Adv. 9 (42) (2019) 24299–24304.
[53] B. Pinho, L. Torrente-Murciano, Continuous manufacturing of silver nanoparticles between 5 and 80 nm with rapid online optical size and shape evaluation, Reaction Chemistry & Engineering 5 (2) (2020) 342–355.
[54] N.T.K. Thanh, N. Maclean, S. Mahiddine, Mechanisms of nucleation and growth of nanoparticles in solution, Chem. Rev. 114 (15) (2014) 7610–7630.
[55] Q.-X. Wang, S.-F. Xue, Z.-H. Chen, S.-H. Ma, S. Zhang, G. Shi, M. Zhang, Dual lanthanide-doped complexes: the development of a time-resolved ratiometric fluorescent probe for anthrax biomarker and a paper-based visual sensor, Biosens. Bioelectron. 94 (2017) 388–393.
[56] D. Kim, S. Kim, H.-T. Ha, S. Kim, Smartphone-based image analysis coupled to paper-based colorimetric devices, Curr. Appl. Phys. 20 (9) (2020) 1013–1018.
[57] T. Qi, M. Xu, Y. Yao, W. Chen, M. Xu, S. Tang, W. Shen, D. Kong, X. Cai, H. Shi, H.K. Lee, Gold nanoprism/Tollens' reagent complex as plasmonic sensor in headspace single-drop microextraction for colorimetric detection of formaldehyde in food samples using smartphone readout, Talanta 220 (2020) 121388.